Journal of Organometallic Chemistry 694 (2009) 3200–3211

Contents lists available at ScienceDirect

Journal of Organometallic Chemistry

journal homepage: www.elsevier.com/locate/jorganchem

Diastereomeric half-sandwich Ru(II) cationic complexes containing amino amide ligands. Synthesis, solution properties, crystal structure and catalytic activity in transfer hydrogenation of acetophenone

Alessia Bacchi, Paolo Pelagatti *, Corrado Pelizzi, Dominga Rogolino

Dipartimento di Chimica Generale ed Inorganica, Chimica Analitica, Chimica Fisica, University of Parma, Viale G.P. Usberti 17/A, 43100 Parma, Italy

ARTICLE INFO

Article history:
Received 9 April 2009
Received in revised form 7 May 2009
Accepted 7 May 2009
Available online 18 May 2009

Keywords:
Ruthenium
Amino amides
Chiral complexes
Configurational stability
Transfer hydrogenation
ESI

ABSTRACT

The cationic complexes [(η^6-arene)Ru(N,O-amino amide)X]Y (arene = p-cymene or indane; N,O-amino amide = (L)-proline amide or (L)-phenylalanine amide; X = Cl or I; Y = Cl, I or PF_6) have been synthesised and fully characterized by spectroscopic and analytical methods. In several cases (**1a**, **3a**, **4a**, **4b**, **5**) the metal configuration has been definitively established by X-ray analysis on single crystal. The lability of the metal center in solution has been studied by ^{1}H NMR and CD techniques. The highest configurational stability has been found in the complexes of the type [(η^6-indane)Ru(N,O-proline amide)Cl]Y (**4a,b**). The complexes **1b**, **2a–b**, **3b**, **4b** and **5** are good precatalysts for the transfer hydrogenation of acetophenone in basic *i*-PrOH, with *ee* up to 76% at 30 °C. An ESI(+)-MS study of pre-catalytic solutions has provided useful information on the catalytic mechanism.

1. Introduction

Half-sandwich ruthenium(II) complexes have shown many interesting properties for a variety of purposes, ranging from catalysis to bioorganometallic chemistry. In recent years, for instance, molecular synthons bearing the (η^6-arene)Ru fragment have been used in the assembly of supramolecular architectures in order to obtain highly selective chemosensors [1]. A great interest has also being devoted to the development of new ruthenium(II) complexes with anticancer activity, where both the arene and the ancillary ligand features are critical in tuning the kinetic of substitution and redox reactions that can occur in a physiological medium [2]. Moreover, compounds of this type with well defined stereochemistries have shown excellent activity in asymmetric catalysis, as nicely exemplified by the transfer hydrogenation of prochiral ketones performed by arene–ruthenium(II) precatalysts containing diamine or amino alcohol ligands [3].

One of the drawbacks of chiral organometallic catalysis is that expensive chiral ligands are often required in order to reach high stereoselectivities. In this context the use of aminoacids appears to be strategic for the creation of inexpensive but still active organometallic catalysts. As regards transfer hydrogenation of ketones, the use of several aminoacids as supporting ligands has been reported by Japanese researchers in 1998 [4] and 2001 [5]. The highest *ee*% were reached with proline and this result was attributed to the higher geometric constrains that the rigid proline imposes onto the Ru–N–C–C(O)–N chelation ring with respect to the other aminoacid precursors. This allows to obtain pure diastereomeric complexes, stable towards epimerization, that can be good enantioselective pre-catalysts, as demonstrated by Noyori for diamine [6] and aminoalcohol ligands [7].

In general, the use of amides of aminoacids as supporting ligands in catalysis is less documented. In 2001 Faller reported on a *in situ* generated (*p*-cymene)Ru(L-proline amide)Cl_2 catalyst that led to enantiomeric excesses up to 93% in the reduction of several ketones at −24 C° [8]. In the same year Chung showed that functionalized proline amide ligands led to *in situ* generated catalysts which showed good enantioselectivities in the reduction of acetophenone, with enantiomeric excesses up to 98.8% [9]. In both cases none detailed information about the nature of the pre-catalyst and active catalyst were reported. Others important contributions on the use of ligands derived from amino acids for the enantioselective reduction of ketones come from Adolfsson's group. Excellent enantioselectivities, up to 98%, were reached with *in situ* formed Ru-precatalysts [10].

Within the framework of our ongoing research program on the development of Ru(II) catalysts for the acetophenone reduction [11], and on the base of the lack of structural information regarding half-sandwich Ru(II) complexes bearing amino amide ligands, in this paper we present the synthesis of a series of cationic complexes of the type {(η^6-arene)Ru[(κ^2NO)-amino amide]X}Y

* Corresponding author. Tel.: +39 0521 905426; fax: +39 0521 905557.
E-mail address: paolo.pelagatti@unipr.it (P. Pelagatti).

0022-328X/$ - see front matter © 2009 Elsevier B.V. All rights reserved.
doi:10.1016/j.jorganchem.2009.05.010

(arene = *p*-cymene or indane; NO-amino amide = (L)-proline amide or (L)-phenylalanine amide; X = Cl, I; Y = Cl, I or PF_6; complexes **1a–4a**, **1b–4b** and **5**). The isolated complexes are depicted in Scheme 1. These have been fully characterized both in solution and in the solid state by NMR, IR, microanalysis, CD and ESI(+)-MS data. The crystalline structures of complexes **1a**, **3a**, **4a–b** and **5** have been determined by diffraction analysis on single crystal, thus unequivocally establishing the metal configuration.

Finally, the complexes **1b**, **2b**, **3b**, **4b** and **5** have been tested as homogeneous pre-catalysts in the transfer hydrogenation of acetophenone in basic *i*-PrOH (KOH as co-catalyst) leading to good catalytic activity and, in some cases, to reasonable enantioselectivities. The ESI(+)-MS characterization of precatalytic solutions indicates that catalysis is governed by a ligand–metal bifunctional mechanism [6].

2. Experimental

2.1. General methods and instruments

All the reactions were carried out under nitrogen, by using standard Schlenk techniques; the solvents were dried according to literature methods and stored over molecular sieves. All reagents of commercial quality were used without further purification. (L)-phenylalanine amide and (L)-proline amide were purchased from Sigma–Aldrich. $[Ru(p\text{-cymene})Cl_2]_2$ [12] and $[Ru(indane)Cl_2]_2$ [13] were prepared by literature reported methods, while $[Ru(p\text{-cymene})I_2]_2$ was purchased by Aldrich. ^1H NMR spectra were recorded on a Bruker Avance 300 FT spectrophotometer or on a Bruker 300 AC spectrophotometer. The chemical shifts are referred to $SiMe_4$. Elemental analyses were performed by using a Carlo Erba Model EA 1108 apparatus. IR spectra were collected with a Nicolet 5PCFT-IR spectrophotometer in the range 4000–400 cm^{-1}, by using KBr pellets or by attenuated total reflection (ATR-diamond crystal). The CD spectra were recorded at 25 °C on a spectropolarimeter Jasco J715 by using 1 cm optical length and 10^{-3} M solutions. The ESI(+)-MS spectra were collected by using a quadrupole-time of flight Micromass spectrometer (Micromass, Manchester, UK) equipped with a pneumatically assisted ESI interface. The systems was controlled by Masslynx software version 4.0 (Micromass). The nebulizing gas (nitrogen, 99.999% purity) and the desolvation gas (nitrogen, 99.998% purity) were delivered at a flow-rate of 10 and 600 L/hr respectively. The interface parameters were: ESI voltage 3.0 kV, cone voltage 5–30 V, rf lens 0.5 V, source temperature 70 °C, desolvation temperature 70 °C. Continuum mode full-scan mass spectra were acquired using an acquisition time of 1 s and an interscan delay of 0.1 s. QqTOF external calibration was performed using a 0.1% phosphoric acid solution and a fifth-order non-linear calibration curve was usually adopted. The GC analyses were performed by means of a Dani-1000 flame ionization gas-chromatograph, equipped with a CP Chirasil Dex CB capillary column (25 m length, 0.25 mm i.d.).

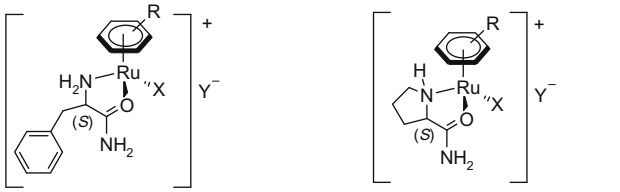

Ar = *p*-cymene, X =Cl, Y = Cl **1a**
Ar = *p*-cymene, X = Cl, Y = PF_6 **1b**
Ar = indane, X =Cl, Y = Cl **3a**
Ar = indane, X = Cl, Y = PF_6 **3b**

Ar = *p*-cymene, X =Cl, Y = Cl **2a**
Ar = p-cymene, X = Cl, Y = PF_6 **2b**
Ar = indane, X =Cl, Y = Cl **4a**
Ar = indane, X = Cl, Y = PF_6 **4b**
Ar = *p*-cymene, X = I, Y = I **5**

Scheme 1. Schematic representation of the synthesised complexes.

2.2. Synthesis

2.2.1. [Ru(η^6-arene)(amino amide)Cl]Cl (**1a–4a**)

0.17 mmol of $[Ru(\eta^6\text{-arene})X_2]_2$ (η^6-arene = η^6-indane or η^6-*p*-cymene) were dissolved in 20 ml of methanol. A methanol solution of the amino amide (proline amide or phenylalanine amide; 0.35 mmol) was slowly added and the resulting solution was stirred at room temperature for 2 h. After filtering over celite, the solvent was removed under vacuum: a foam was obtained, which was triturated with CH_2Cl_2/*n*-hexane in order to isolate a powder.

2.2.2. [Ru(η^6-arene)(amino amide)Cl]PF_6 (**1b–4b**)

0.17 mmol of $[Ru(\eta^6\text{-arene})Cl_2]_2$ (η^6-arene = η^6-indane or η^6-*p*-cymene) were dissolved in 20 ml of dichloromethane. A solution of the amino amide (0.35 mmol) in dichloromethane was slowly added and the resulting solution was stirred at room temperature for 30 min. KPF_6 (0.4 mmol) was added and the solution stirred for additional 4 h. After filtering over celite, the solvent was removed under vacuum: the crude residue was triturated with *n*-hexane in order to obtain a powder.

2.2.3. [Ru(η^6-*p*-cymene)ProI]I (**5**)

0.25 mmol of $[Ru(\eta^6\text{-}p\text{-cymene})I_2]_2$ and 0.50 mmol of L-prolinamide were dissolved in 20 ml of *i*-PrOH and the resulting purple solution was refluxed for 3 h. After a night at room temperature the solution released a gold–brown microcrystalline solid, which was filtered off, recrystallized in a methanol/diethyl ether mixture. The red–brown crystals were filtered, washed with diethyl ether and finally vacuum dried.

2.2.4. [Ru(η^6-*p*-cymene)PhalaCl]Cl, **1a**

Brown powder. Yield: 75%. IR (KBr, cm^{-1}): 3061–3298 (NH); 1653 (C=O). Anal. calc. for $C_{19}H_{26}Cl_2N_2ORu$: C 48.51; H 5.57; N 5.95. Found: C 48.47; H 5.45; N 5.68. ^1H NMR (CD_3OD): major diastereoisomer δ 1.31 (t, br, partly overlapped signals, CH_3); 2.11 (s, 3H, CH_3); 2.77 (m, partly overlapped signals); 3.00–3.21 (m, partly overlapped signals); 3.82 (m, br, 1H, *CH); 5.58 (d, 2H, H_{cym}); 5.75 (d + s, 3H, H_{cym} + NH); 7.34–7.45 (m, H_{arom}, partly overlapped signals). Minor diastereoisomer: δ 2.16 (s, 3H, CH_3); 4.03 (m, 1H, *CH); 5.36 (d, 2H, H_{cym}); 5.67 (d, 2H, H_{cym}). Recrystallization from ethanol afforded crystals suitable for X-ray analysis.

2.2.5. [Ru(η^6-*p*-cymene)PhalaCl]PF_6, **1b**

Orange powder. Yield: 73%. IR (KBr, cm^{-1}): 3089–3268 (NH); 1655 (C=O); 844 (PF_6). Anal. calc. for $C_{19}H_{26}ClF_6N_2OPRu{\cdot}1.5\,CH_2Cl_2$: C 34.81; H 4.13; N 3.95. Found: C 34.43; H 4.02; N 3.92. ^1H NMR (CD_3OD): major diastereoisomer δ 1.30 (t, br, partly overlapped signals, CH_3); 2.10 (s, 3H, CH_3); 2.71–2.85 (m, partly overlapped signals); 2.97–3.25 (m, partly overlapped signals); 3.81–3.86 (m, br, 1H, *CH); 5.28 (d, 1H, H_{cym}); 5.60–5.65 (m, 2H, NH + H_{cym}); 5.87 (d, 2H, H_{cym}); 7.31–7.53 (m, H_{arom}, partly overlapped signals). Minor diastereoisomer: δ 2.16 (s, 3H, CH_3); 4.02 (m, 1H, *CH); 5.28 (d, 2H, H_{cym}); 5.75 (d, 2H, H_{cym}).

2.2.6. [Ru(η^6-*p*-cymene)ProCl]Cl, **2a**

Ochre powder. Yield 78%. IR (KBr, cm^{-1}): 3112–3316 (NH); 1652 (C=O). Anal. calc. for $C_{15}H_{24}Cl_2N_2ORu{\cdot}0.25CH_2Cl_2$: C 41.48; H 5.59; N 6.34. Found: C 41.69; H 5.89; N 6.06. ^1H NMR (CD_3OD): major diastereoisomer δ 1.34 (d, 6H, CH_3); 1.75–1.79 (m, 2H); 2.01–2.03 (m, 1H); 2.23 (s, 3H, CH_3); 2.41–2.45 (m, 1H); 2.81–2.90 (m, 1H); 3.30–3.32 (m, 1H); 3.40–3.42 (m, 1H); 3.85 (dd, 1H, NH); 4.03 (dd, br, 1H, *CH); 5.55 (d, 1H, H_{cym}); 5.68–5.72

(d, 2H, H_{cym}); 5.84 (d, 1H, H_{cym}). Minor diastereoisomer: δ 1.38 (d, 6H, CH_3); 2.19 (s, 3H, CH_3); 5.63 (d, 2H, H_{cym}); 5.77 (d, 2H, H_{cym}).

2.2.7. [Ru(η^6-p-cymene)ProCl]PF_6, ***2b***

Yellow powder. Yield: 79%. IR (KBr, cm^{-1}): 3107–3288 (NH); 1654 (C=O); 841 (PF_6). Anal. calc. for $C_{15}H_{24}ClF_6N_2OPRu{\cdot}2CH_2Cl_2$: C 29.18; H 4.32; N 4.00. Found: C 29.24; H 3.99; N 4.40. ^{1}H NMR (CD_3OD): major diastereoisomer δ 1.31–1.39 (dd, partly overlapped signals, CH_3); 1.75–1.83 (m, 2H); 2.04–2.08 (m, 1H); 2.22 (s, 3H, CH_3); 2.42 (m, 1H); 2.83–2.87 (m, 1H); 3.25–3.33 (m, 2H); 3.85 (dd, 1H, NH); 4.04 (dd, br, 1H, *CH); 5.57 (d, 1H, H_{cym}); 5.67–5.73 (d + d, 2H, H_{cym}); 5.83 (d, 1H, H_{cym}). Minor diastereoisomer: δ 2.18 (s, 3H, CH_3); 5.59 (d, 2H, H_{cym}); 5.78 (d, 2H, H_{cym}).

2.2.8. [Ru(η^6-indane)PhalaCl]Cl, ***3a***

Yellow powder. Yield: 75%. IR (KBr, cm^{-1}): 3060–3299 (NH); 1652 (C=O). Anal. calc. for $C_{18}H_{22}Cl_2N_2ORu{\cdot}\ 0.5CH_2Cl_2$: C 45.93; H 4.66; N 5.63. Found: C 46.25; H 4.48; N 5.90. ^{1}H NMR (CD_3OD): major diastereoisomer δ 2.16–2.25 (m, partly overlapped signals); 2.65–2.82 (m, partly overlapped signals); 2.97 (dd, 1H); 3.08 (dd, 1H); 3.23 (dd, 2H); 3.83 (dd, 1H, *CH); 5.59–5.70 (m, partly overlapped signals, H_{indane}); 7.31–7.35 (m, partly overlapped signals, H_{arom}). Minor diastereoisomer: δ 4.04 (dd, 1H, *CH); 5.40 (t, 2H, H_{indane}); 5.59 (t, 1H, H_{indane}); 5.83 (d, 1H, H_{indane}), 5.86 (s, br, NH). Recrystallization from nitromethane afforded crystals suitable for X-ray analysis.

2.2.9. [Ru(η^6-indane)PhalaCl]PF_6, ***3b***

Yellow powder. Yield: 82%. IR (KBr, cm^{-1}): 3332–3368 (NH); 1656 (C=O); 841 (PF_6). Anal. calc. for $C_{18}H_{22}ClF_6N_2OPRu$: C 38.40; H 3.76; N 4.97. Found: C 38.27; H 4.12; N 4.76. ^{1}H NMR (CD_3OD): major diastereoisomer δ 2.14–2.19 (m, partly overlapped signals); 2.65–2.73 (m, partly overlapped signals); 2.88–2.91 (m, 1H); 3.07–3.10 (m, 1H); 3.21 (dd, 2H); 3.86 (dd, 1H, *CH); 5.58–5.68 (m, partly overlapped signals, H_{indane}); 7.35–7.42 (m, partly overlapped signals, H_{arom}). Minor diastereoisomer: δ 4.04 (dd, 1H, *CH); 5.37 (t, 2H); 5.40 (t, 1H, H_{indane}); 5.72 (d, 1H, H_{indane}).

2.2.10. [Ru(η^6-indane)ProCl]Cl, ***4a***

Yellow powder. Yield: 60%. IR (KBr, cm^{-1}): 3257 (NH); 1655 (C=O). *Anal.* calc. for $C_{14}H_{20}Cl_2N_2ORu$: C 41.59; H 4.98; N 6.92. Found: C 41.49; H 4.98; N 6.38. ^{1}H NMR (CD_3OD): δ 1.72–1.76 (m, 2H); 2.04–2.41 (m, 4H); 2.71–2.76 (m, 2H); 2.83–2.96 (m, 2H); 3.20 (m, 1H); 3.41 (m, 1H); 3.88 (t, br, 1H, *CH); 4.02 (dd, 1H, NH); 5.58–5.61 (m, 1H, H_{indane}); 5.72–5.78 (m, 3H, H_{indane}); 5.89 (s, br, NH). Minor diastereoisomer: δ 4.29 (dd, 1H, *CH) Recrystallization from methanol/ethanol afforded crystals suitable for X-ray analysis.

2.2.11. [Ru(η^6-indane)ProCl]PF_6, ***4b***

Orange powder. Yield: 80%. IR (KBr, cm^{-1}): 3068–3266 (NH); 1657 (C=O); 836 (PF_6). Anal. calc. for $C_{14}H_{20}ClF_6N_2OPRu{\cdot}\ 2CH_2Cl_2$: C 28.11; H 3.53; N 4.09. Found: C 28.07; H 3.18; N 4.29. ^{1}H NMR (CD_3OD): δ 1.72–1.80 (m, 2H); 2.04–2.41 (m, 4H); 2.69–2.98 (m, 4H); 3.25 (m, 2H); 3.86 (m, br, 1H, *CH); 3.98 (m, br, 1H, NH); 5.59–5.62 (m, 1H, H_{indane}); 5.71–5.77 (m, 3H, H_{indane}); 5.86 (s, br, NH). Recrystallization from acetone and from water afforded crystals suitable for X-ray analysis.

2.2.12. [Ru(η^6-p-cymene)ProI]I, ***5***

Purple solid. Yield: 75%. IR (ATR, diamond, cm^{-1}): 3140–3400 (NH), 1658 (C=O). Anal. calc. for $C_{15}H_{24}I_2N_2ORu$: C 30.25; H 4.44; N 4.41. Found: C 29.87; H 4.18; N 4.36. ^{1}H NMR (CD_3OD): major diastereoisomer δ 1.30 (d, 3H, CH_3), 1.35 (d, 3H, CH_3), 1.72–1.83 (m, 2H, CH_2), 2.02–2.06 (m, 2H, CH_2), 2.21 (s, 3H, CH_3), 2.31–2.40 (m, 1H, CH_2), 2.81–2.90 (m, 1H, CH), 3.23–3.31 (m, 2H, NCH_2), 3.88–3.96 (dd, 1H, NH), 4.00–4.05 (dd, 1H, *CH), 5.60 (d, 1H, CH_{cym}), 5.76 (d, 1H, CH_{cym}), 5.81 (d, 1H, CH_{cym}), 5.94 (d, 1H, CH_{cym}). Minor diastereoisomer: δ 1.25 (d, 3H, CH_3, partially overlapped signals), 2.25 (s, 3H, CH_3), 3.75 (m, 1H, NH), 4.27 (m, 1H, CH).

2.3. X-ray structures determination

MoKα radiation (λ = 0.71073 Å) on a SMART AXS 1000 CCD diffractometer for **1a**, **3a** and **4a**, on a Philips PW100 diffractometer for **4b** and on a Bruker AXS APEX2 for **5**. All data were collected at room temperature (293 K). Lorentz, polarization, and absorption corrections were applied [14]. Structures were solved by direct methods using SIR97 [15] and refined by full-matrix least-squares on all F^2 using SHELXL97 [16] implemented in the WingX package [17]. Hydrogen atoms partly located on Fourier difference maps and refined isotropically and partly introduced in calculated

Table 1
Crystal data and structure refinement for **1a**, **3a** and **4a**.

	1a	3a	4a
Empirical formula	$C_{19}\ H_{26}\ Cl_2\ N_2\ O\ Ru$	$C_{18}\ H_{24}\ Cl_2\ N_2\ O_2\ Ru$	$C_{14}\ H_{20}\ Cl_2\ N_2\ O\ Ru$
Formula weight	470.39	472.36	404.29
Wavelength (Å)	0.71073	0.71073	0.71073
Crystal system	Triclinic	Monoclinic	Monoclinic
Space group	*P* 1	$P\ 2_1$	$P\ 2_1$
Unit cell dimensions (Å, °)	*a* = 7.6168(4)	*a* = 9.5370(5)	*a* = 6.6547(5)
	α = 81.495(1)	*b* = 7.8896(4)	*b* = 11.0421(8)
	b = 9.4338(6)	β = 108.435(1)	β = 100.934(1)
	β = 87.608(1)	*c* = 13.6567(7)	*c* = 10.6985(8)
	c = 14.8927(9)		
	γ = 87.167(1)		
Volume ($Å^3$)	1056.4(1)	974.84(9)	771.9(1)
Z	2	2	2
Density (calculated) (Mg/m^3)	1.479	1.609	1.740
Absorption coefficient (mm^{-1})	1.004	1.092	1.358
F(0 0 0)	480	480	408
Reflections collected	13358	8966	9269
Independent reflections	9837 [R_{int} = 0.0260]	4470 [R_{int} = 0.0171]	3626 [R_{int} = 0.0206]
Data/restraints/parameters	9837/3/409	4470/4/234	3626/3/253
Goodness-of-fit on F^2	0.775	1.002	1.023
Final *R* indices [$I > 2\sigma(I)$]	R_1 = 0.0417, wR_2 = 0.0730	R_1 = 0.0245, wR_2 = 0.0617	R_1 = 0.0196, wR_2 = 0.0484
R indices (all data)	R_1 = 0.0840, wR_2 = 0.0814	R_1 = 0.0267, wR_2 = 0.0627	R_1 = 0.0206, wR_2 = 0.0489
Absolute structure parameter	0.01(5)	−0.05(3)	0.01(2)
ΔF maximum/minimum (e $Å^{-3}$)	0.585/−0.270	0.304/−0.418	0.373/−0.407

positions. Anisotropic displacement parameters refined for all non-hydrogen atoms. Hydrogen bonds have been analyzed with SHELXL97 [16] and PARST97 [18], and extensive use was made of the Cambridge Crystallographic Data Center packages [19]. Table 1 summarizes crystal data and structure determination results for **1a**, **3a** and **4a**, while the data of complexes **4b** and **5** are reported in the Supplementary data.

2.4. Catalytic transfer hydrogenation

2.4.1. Catalytic tests conducted with the preformed complexes

5 mg of the complex were carefully weighed and placed in a 100 ml capacity Schlenk tube equipped with a magnetic bar, which was evacuated by vacuum pump and refilled with nitrogen at least three times. *i*-PrOH was then transferred by syringe and the resulting solution was thermostated at the desired temperature (20, 30, 40 or 82 °C). Then acetophenone (Ru:acetophenone molar ratio = 1:200) and the necessary volume of a 0.34 M KOH/*i*-PrOH solution (Ru:KOH molar ratio = 1:2) were added under stirring. The final Ru concentration was 10^{-4} M, while the final acetophenone concentration was 0.1 M. Three subsequent samples (0.5 mL) were withdrawn after 30, 60 and 90 min. Each sample was passed through a short silica column in order to remove the metal (diethyl ether as eluent), then treated with water and extracted three times with diethyl ether. After drying with anhydrous sodium sulfate and filtering, the samples were analyzed by GC.

2.4.2. Catalytic tests conducted with the in situ generated catalysts

Carefully weighed amounts of free ligand and $[Ru(\eta^6\text{-arene})X_2]_2$ (molar ratio = 2:1) were placed in a 100 ml capacity Schlenk tube equipped with a magnetic bar, which was evacuated by vacuum pump and refilled with nitrogen at least three times. *i*-PrOH was then transferred by syringe and the resulting solution was stirred at room temperature for at least thirty minutes. The Ru and acetophenone concentrations were 10^{-4} and 0.1 M, respectively. Then the procedure was as previously reported.

2.5. ESI-MS experiments

The solutions were prepared as described for the catalytic runs. Aliquots of the reactant solutions were withdrawn and immediately analyzed by direct infusion into the ESI source equipped with a Qq-TOF high resolution MS spectrometer. All the experimental isotope clusters were in agreement with the theoretical masses and with the reconstructed singly charged ESI isotope patterns.

3. Results and discussion

3.1. Synthesis of the ruthenium complexes and solution properties

The title complexes (Scheme 1) have been prepared by reacting the appropriate $[Ru(arene)X_2]_2$ dimer with two equivalents of amino amide ligand in methanol at room temperature (**1a**–**4a**) or in refluxing *i*-PrOH (**5**). The synthesis of complex **2a** has already been reported by Beck and co-workers [20], while the other complexes have not yet been described in the literature. The corresponding **1b**–**4b** analogs, containing the uncoordinated PF_6^- anion in place of the Cl^- one, have been obtained by reacting *in situ* the ligand, the chloride dimer and KPF_6 in dichloromethane at room temperature. The complexes have been isolated as yellow–orange powders (**1a**–**4a** and **1b**–**4b**) or red crystals (**5**) in high yields. They show good solubility in alcoholic solvents, acetone and water. Their full characterization has been obtained by ^{1}H NMR, IR and CD spectroscopy, ESI-MS and elemental analysis. In several cases (**1a**, **3a**, **4a**, **4b** and **5**) the solid structure has been solved by X-ray diffraction analysis on a single crystal.

The data clearly indicate that the amino amides behave as neutral bidentate ligands, giving rise to pseudo-octahedral organometallic cations of formula $\{(\eta^6\text{-arene})Ru[(\kappa^2NO)\text{-amino amide}]X\}^+$ (arene = *p*-cymene or indane; NO-amino amide = L-proline amide or L-phenylalanine amide; X = Cl or I), whose charge is neutralized by an uncoordinated Cl^- (**1a**–**4a**), PF_6^- (**1b**–**4b**) or I^- (**5**) anion. L-proline amide and L-phenylalanine amide coordinate the metal in a NO fashion, as confirmed by X-ray diffraction analysis on single crystals. This way of coordination differs from that observed in the neutral complexes $\{(\eta^6\text{-}p\text{-cymene})Ru[(\kappa^2NN')\text{-amino amidato}]Cl\}$ (NN′-amino amidato = L-phenylalanine amidato, L-phenylalanine-*p*-anisidineamidato, L-valine-*o*-anisidineamidato) [11a,b], which were synthesised in the presence of a stoichiometric amount of base. In these cases the deprotonation of the amide function forced the ligand to bind ruthenium in a NN′ mode [21]. The coordination isomerism of the amide group can be suitably monitored by IR spectroscopy. In fact, in the IR spectrum of **1a**–**4a**, **1b**–**4b** and **5** it is possible to observe the intense absorption of the coordinated C=O group at around 1650 cm^{-1}, while in the neutral amino amidato complexes the band of the same uncoordinated group shifts to 1580 cm^{-1} [11a,b]. In the complexes **1a**–**4a**, **1b**–**4b** and **5** the coordination through the oxygen does not however significantly affects the IR absorption with respect to those found for the free ligands, which fall in the range 1655–1668 cm^{-1}. The Cl^-/PF_6^- anion substitution can be easily inferred by IR spectra, where the stretching of the PF_6^- anion is visible at around 830 cm^{-1}. The anion substitution has further been confirmed by elemental analysis and X-ray diffraction (*vide infra*).

The progress of the reactions between free L-proline amide and L-phenylalanine amide with $[Ru(p\text{-cymene})Cl_2]_2$ and $[Ru(indane)Cl_2]_2$ in methanol at room temperature has been monitored by ESI-MS analysis. The full conversion of the reagent is accomplished after a few minutes of reaction. The ESI-MS spectra collected with a CV = 5 V show as predominant signal the cluster corresponding to the cation $\{(\eta^6\text{-arene})Ru[(\kappa^2NO)\text{-amino amide}]Cl\}^+$ [m/z = 435 (**1a**), m/z = 385 (**2a**), m/z = 419 (**3a**), m/z = 369 (**4a**)]. Another much less intense signal is that belonging to the coordinatively unsaturated amino-amidato species $\{(\eta^6\text{-arene})Ru[(\kappa^2NN')\text{-amino amidato}]\}^+$[m/z = 429 (**1a**), m/z = 349 (**2a**), m/z = 383 (**3a**), m/z = 333 (**4a**)]. The formation of such species occurs in the gas phase through HCl elimination, as evidenced by the growing of the same signal at higher CV values, becoming the most intense signal at a CV = 30 V (Scheme 2).

The pseudo-octahedral complexes **1a**–**4a**, **1b**–**4b** and **5** contain an enantiomerically pure ligand and can, in principle, form two diastereoisomers differing for the metal configuration, $R_{Ru}S_c$ and $S_{Ru}S_c$. Usually, ligands such as aminoacidates or amino amidates give rise to two diastereoisomers, that show epimerization at the metal center in solution [11a,b,22]. If the interconvertion of the two diastereoisomers occurs slowly on the NMR-time scale, two sets of signals can be observed. In the title compounds the two different isomers can be distinguished by several diagnostic signals, such as those belonging to the CH_3 group of the *p*-cymene moiety at about 2.1 ppm, the multiplets belonging to the *CH moiety of the amino amide ligand in the region 3.8–4.3 ppm and by means of the doublets belonging to the η^6-coordinated arene in the region 5.3–5.8 ppm (see Section 2). From the NMR integrals the diastereomeric ratio can then be inferred.

The ^{1}H NMR spectrum of **1a** recorded in methanol at room temperature shows two sets of well resolved signals, thus indicating the coexistence of both diastereoisomers in a 33/67 ratio. The proton spectrum recorded after having maintained the solution at room temperature for 24 h shows an unchanged diastereomeric ratio, thus indicating that the thermodynamic equilibrium between

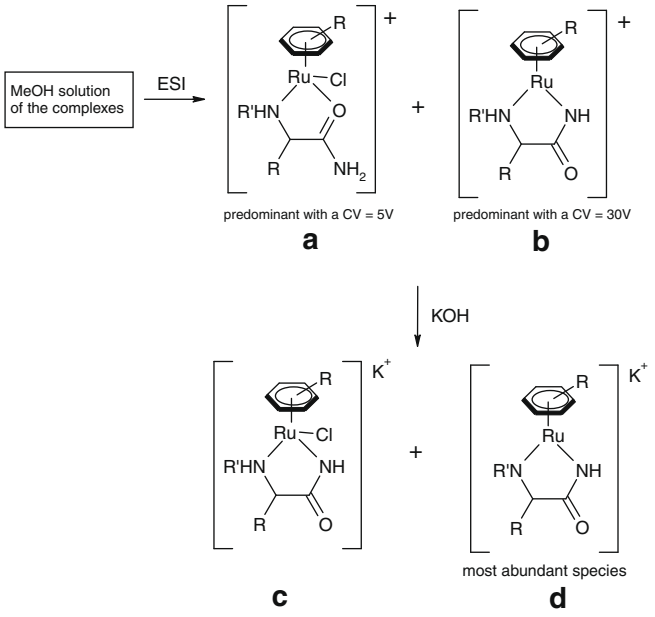

Scheme 2. ESI(+)-MS characterization of the Ru-complexes.

the two isomers is reached immediately after dissolution. The X-ray analysis conducted on a single crystal of **1a** grown in ethanol evidences the co-crystallization of the two diastereoisomers in a "inverted-piano stool"-like motif [11a,23] (*vide infra*), to say in a 50/50 ratio. Once dissolved in deuterated methanol at room temperature, the crystals give rise to a ^{1}H NMR spectrum with a 33/67 diastereomeric ratio, thus pointing out that in solution a fast epimerization at metal occurs. The hexafluorophosphate **1b** shows the same feature.

The ^{1}H NMR spectra of **2a–b** recorded in deuterated methanol or acetone at room temperature reveal the presence of the two diastereoisomers in a 25/75 ratio, ratio which does not change with time. This result differs from that previously reported by Beck in $CDCl_3$ [20], corresponding to a 11:89 ratio. The found difference suggests that the epimerization occurs through chloride detachment, which is expected to be favored in polar coordinating solvents such as those used in the present work. This suggestion is further corroborated by the behavior shown by **2a** in D_2O (*vide infra*). Unfortunately, in both cases, it has not been possible to grow single crystals suitable for X-ray analysis. However, the crystal structure of **5** solved by X-ray diffraction on a single crystal grown in a methanol/*n*-hexane mixture evidences only the $S_{Ru}S_C$ diastereoisomer (see Supplementary data). The ^{1}H NMR spectrum of the crystals of **5** dissolved in deuterated methanol at room temperature shows a 9:91 diastereomeric ratio. The ratio remains unchanged within 24 h at room temperature, thus pointing out that with X = Y = I the epimerization process is strongly unfavored.

The ^{1}H NMR spectra of the complexes **3a–b** recorded in deuterated methanol at room temperature show a 33/67 diastereomeric ratio, equivalent to that observed for the complexes containing the *p*-cymene ring **1a**–**b**. The ratio does not change with time on standing the solution at room temperature. Complex **3a** crystallizes as a unique diastereoisomer ($R_{Ru}S_C$) as indicated by X-ray diffraction on a single crystal grown in nitromethane (*vide infra*). Dissolution of the crystals of **3a** in deuterated methanol at room temperature leads to the restoration of the 33/67 ratio, as established by ^{1}H NMR spectroscopy, thus indicating the occurrence of epimerization at metal.

The ^{1}H NMR spectra of the complexes **4a–b** show, in deuterated methanol and room temperature, a 15/85 diastereomeric ratio. As above, the ratio remain unchanged at room temperature with time. Complexes **4a–b** crystallize as a unique diastereoisomer ($S_{Ru}S_C$) in a ethanol/methanol mixture and acetone, respectively (*vide infra*). With both complexes the solutions obtained dissolving the crystals in deuterated methanol at room temperature show ^{1}H NMR spectra containing a single set of signals, which do not change on standing the samples at room temperature for 48 h. The NMR spectra of the crystals show that the $S_{Ru}S_C$ isomer was the most abundant in the initial mixture.

The CD spectrum of crystals of **4a** has been recorded in methanol at room temperature. The spectrum shows a negative Cotton effect centered at 366 nm, followed by a positive one centered at 435 nm, which is therefore associated to the $S_{Ru}S_C$ configuration as established by X-ray diffraction analysis (see Supplementary data). The spectrum remains unaltered for several days, pointing out the absence of any epimerization occurring at room temperature, in agreement with the NMR observations. The CD spectra of the complexes **1a, 2a** and **3a** under the same conditions show similar patterns, indicating that in solution the S_{Ru} configuration predominates (see Supplementary data). Again, the spectra do not change with time, as already established by NMR spectroscopy. On the basis of the X-ray result and stability we can assign the $S_{Ru}S_C$ configuration for the most abundant isomer of **5** as well. These assumption are further corroborated by the very similar enantioslectivities shown in catalysis by **2a–b** and **5** (*vide infra*).

The solubility of the title complexes in water makes them attractive for bioorganometallic applications and catalysis in water media. In order to get insights into their behavior in water the ^{1}H NMR spectra of the complexes **1a–4b** have been collected in deuterated water at room temperature. In the case of **1a**, **2a** and **3a** a broadening effect is visible, which points out a faster epimerization with respect to that observed in methanol, the diastereomeric ratio resulting roughly the same. In neutral half-sandwich complexes containing salicyloxazoline ligands the same broadening effect has been observed after the addition of water into dichloromethane solutions of the complexes and it has been ascribed to the loss of the chloride ion upon coordination of a water molecule [24]. This seems confirmed also for **1a**–**3a,** since sharp signals have been obtained in the protonic spectrum of **1a** recorded in D_2O at room temperature after the addition of an excess of NaCl. A different situation is found for **4a** and **4b** which show sharp signals also in deuterated water, the diastereomeric ratio being the same found in deuterated methanol. This is in accord with the observation that such complexes do not epimerize in solution, as discussed above. In fact, recrystallization of **4b** in water leads to diastereomerically pure crystals having the $S_{Ru}S_C$ configuration, as found in methanol.

A rationalization of the different effects determining the stereochemical outcome for the ruthenium complexes can be given. In the case of the chloride complexes L-proline amide exerts a higher stereochemical control than L-phenylalanine amide, leading in general to higher diastereomeric excesses. This is in agreement with the recognized ability of proline amide to generate effective organometallic catalysts [8–9] as well as organocatalysts [25]. The effect of the arene ligand seems to depend on the amino amide ligand. In fact, the diastereomeric excess found in the solutions of complexes **1** and **3** are equivalent, pointing out that for L-phenylalanine amide the two arene rings are equivalent. With L-proline amide instead, a slight increment of the dsiastereoselectivity is observed on passing from complexes **2** (*p*-cymene) to complexes **4** (indane). However, the nature of the arene ligand seems to influence more profoundly the stereochemical outcome in the solid state. With L-phenylalanine amide and *p*-cymene the diastereomeric mixture found in solution leads to crystals containing a perfect racemate. This sort of molecular recognition is based on inverted piano-stool dimers [23] and it has recently been observed by us in (*p*-cymene)Ru(II)-complexes containing amino amidato

ligands [11a,b]. In the presence of indane L-phenylalanine amide leads instead to the selective crystallization of the $R_{Ru}S_C$ diastereoisomers. The different behavior can be ascribed to the high steric encumbrance created by indane, which hampers the formation of the intermolecular hydrogen bond network necessary for the construction of the inverted piano-stool dimers [23]. Worth of mention is that the metal configuration found in the X-ray structure of **3a** (R_{Ru}) is opposite to those found in the diastereomeric pure crystals of **4a–b** (S_{Ru}). On the basis of the CD results we can conclude that in the case of **3a** the fractional crystallization leads to the faster formation of the less abundant isomer $R_{Ru}S_C$.

Importantly, the combination L-proline amide/indane leads to configurationally stable diastereoisomers, as evidenced by complexes **4a**–**4b**. In this context, the presence of indane appears crucial, as evidenced by the epimerization observed with the configurationally pure crystals of complex **5**. In this case however, the effect of the halogen cannot be ignored.

3.2. X-ray structures

The crystal structure of **1a** (Fig. 1) comprises two independent diastereoisomeric {Ru[(η^6-*p*-cymene)phenylalanine amide]Cl}$^+$ cations which cocrystallize in the purely translational P1 space group together with two corresponding chloride counteranions. In both cases ruthenium is pseudo-octahedrally coordinated to the chlorine ligand, the nitrogen and the oxygen atoms of the bidentate aminoamidic ligand and the *p*-cymene aromatic ring. The most relevant geometric features are reported in Table 2. The absolute configuration on the metal is opposite for Ru1 (*R*) and Ru2 (*S*), while the chirality of the optically active carbon on the phenylalanine ligand is always the same. The absolute configuration of the cations is thus $R_{Ru1}S_C$ and $S_{Ru2}S_C$ respectively, and the combination of the two chiral centers produces different local arrangements on the two molecules. In the coordination sphere the Ru-O bond appears significantly longer for the $R_{Ru1}S_C$ isomer, whereas the remaining bonds are similar. In both cases the *p*-cymene methyl group is eclipsed to the Ru-O bond (C7–C4–Ru1–O1 = 2°, C26–C20–Ru2–O2 = 0°) and the *i*-propyl is staggered between the Ru–Cl and the Ru–N bonds (C8–C1–Ru1–Cl1 = 38°, C8–C1–Ru1–N1 = −48°; C27–C23–Ru2–Cl2 = −34°, C27–C23–Ru2–N4 = 52°), while phenylalanine orientation and conformation are affected by the combination of the two chiral centers at Ru and C. In the $S_{Ru2}S_C$ complex the CH bond at the chiral center is *syn* to the Ru2–Cl2 bond, while in the $R_{Ru1}S_C$ cation the CH is oriented on

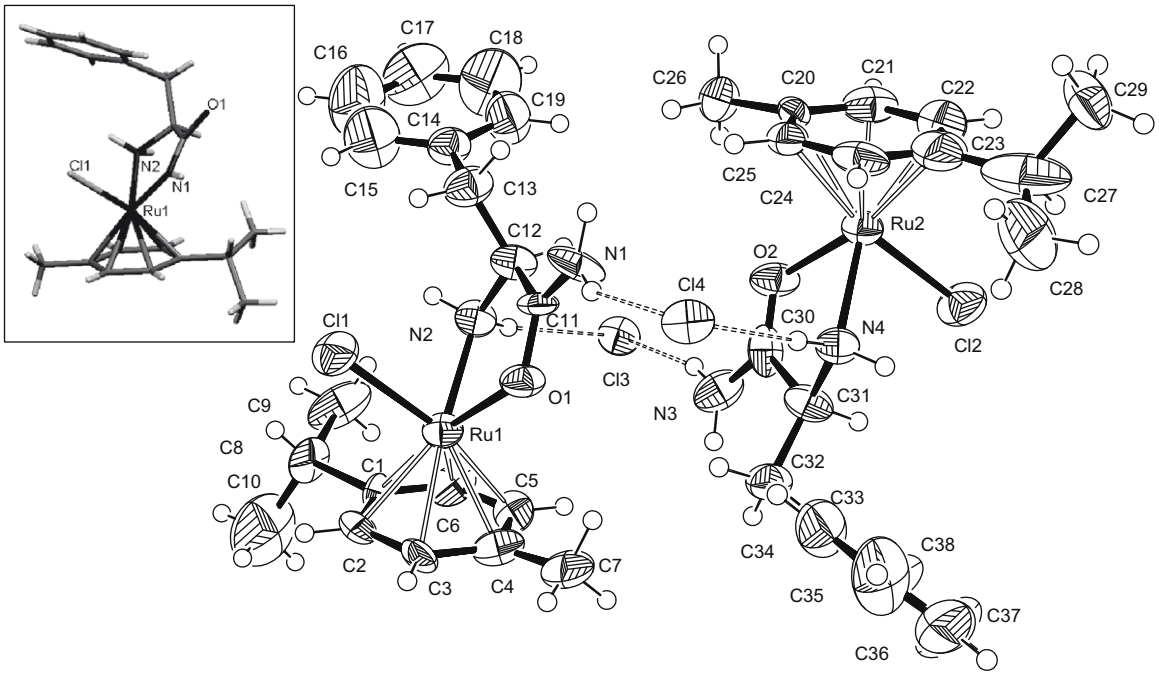

Fig. 1. Perspective view and labeling scheme of the pair of diastereoisomeric complexes in the crystal structure of **1a**. Hydrogen bonds are shown as dashed lines. Thermal ellipsoids at the 50% probability level. Inset: comparison with the molecular structure of the $R_{Ru1}S_C$ isomer of the neutral complex {Ru[(η^6-*p*-cymene)(κ^2N,O-phenylalanine amide)Cl}[11a].

Table 2
Principal bond distances and angles (Å, °) for the coordination geometry of **1a**, **3a** and **4a**. CM denotes the centroid of the η^6 coordinated arene rings. E.s.d.'s in parentheses.

1				**3a**		**4a**	
Ru1–N2	2.14(1)	Ru2–N4	2.13(1)	Ru1–N1	2.142(3)	Ru1–N2	2.149(2)
Ru1–O1	2.146(8)	Ru2–O2	2.095(9)	Ru1–O1	2.109(2)	Ru1–O1	2.092(2)
Ru1–Cl1	2.406(4)	Ru2–Cl2	2.394(4)	Ru1–Cl1	2.4228(6)	Ru1–Cl1	2.4184(7)
Ru1–CM1	1.66	Ru2–CM2	1.64	Ru1–CM	1.65	Ru1–CM	1.67
N2–Ru1–O1	76.4(4)	O2–Ru2–N4	76.5(4)	O1–Ru1–N1	77.73(9)	O1–Ru1–N2	78.67(7)
N2–Ru1–Cl1	83.3(3)	N4–Ru2–Cl2	82.9(3)	N1–Ru1–Cl1	84.00(8)	O1–Ru1–Cl1	82.85(6)
O1–Ru1–Cl1	86.6(3)	O2–Ru2–Cl2	88.2(3)	O1–Ru1–Cl1	88.21(8)	N2–Ru1–Cl1	83.61(6)
CM1–Ru1–Cl1	127.6	CM2–Ru2–Cl2	129.8	CM–Ru1–Cl1	130.0	CM–Ru1–Cl1	130.0
CM1–Ru1–O1	132.0	CM2–Ru2–O2	126.8	CM–Ru1–O1	126.5	CM–Ru1–O1	128.5
CM1–Ru1–N2	132.5	CM2–Ru2–N4	134.4	CM–Ru1–N2	132.8	CM-Ru1-N2	134.1

the opposite side. According to the Cremer and Pople puckering descriptors [26] the chelation ring is significantly more puckered and twisted in the former case ($q2 = 0.36(1)$ Å^2, $\varphi2 = -28(2)°$) than in the latter ($q2 = 0.20(1)$ Å^2, $\varphi2 = 179(3)°$). This analysis evidences that the two diastereoisomeric cations present a pseudo centric symmetry that relates the coordination cores, frustrated by the optical purity of the amino amidic ligand that prevents the formation of a genuine centrosymmetric molecular pair. The crystallization of two concomitant diastereoisomers related by a pseudo centric symmetry, the so-called inverted piano-stools pair, is characteristic of this family of half-sandwich molecules [11a] and refers to the high efficiency of the center of inversion in favoring the close packing in the solid state [27]. The inverted piano-stool pattern is usually based on the direct short range interaction of pairs of neutral molecules [23], while in this case the diastereoisomeric cations are bridged by the chloride counteranions in a pseudo centric dimer $[R_{Ru1}S_C\ S_{Ru2}S_C]Cl_2$ assembled through hydrogen bonds involving the amidic $-NH_2$ (N1–H···Cl4 = 3.20(1) Å, 154.3(7)°, N1–H···Cl3 $(x-1,\ y,\ z)$ = 3.26(1) Å, 140.0(7)°; N3–H···Cl3 = 3.20(1) Å, 164.4(7)°, N3–H···Cl4 $(x+1,\ y,\ z)$ = 3.27(1) Å, 141.5(7)°). The packing (Fig. 2) is thus based on strands of cationic chains bridged by chloride anions built by translation along ***a***, while the amidic oxygen and the second hydrogen of the aminic NH_2 are not employed. The structure of **1a** can be compared to the corresponding neutral complex {Ru[(η^6-*p*-cymene)phenylalanine amide]Cl} [11a] (Fig. 1, inset), where the amino amidic ligand is deprotonated. In that case the coordination of phenylalanine occurred by N,N′ chelation, and the *p*-cymene was oriented with the methyl group *syn* to the chloride, *i.e.* rotated by about 150° compared to **1a**.

3a has been isolated as a crystalline material in its monohydrate form, {Ru[(η^6-indane) phenylalanine]Cl}Cl·H_2O. The cation, shown in Fig. 3, is obtained as a unique isomer with configuration $R_{Ru}S_C$, whereas the analogous *p*-cymene complex **1a** crystallizes as a diastereoisomeric pair as discussed above. Coordination bonds and angles in **3a** differ significantly form those observed for **1a**, as reported in Table 2. In particular, the Ru–Cl bond distance is significantly longer in the indane complex, while the coordination to phenylalanine and to the arene is comparable with the one observed in **1a** for the $S_{Ru2}S_C$ isomer. The chelation ring is slightly less puckered than in **1a** ($q2 = 0.18(1)$ Å^2, $\varphi2 = 86(1)°$). The indane five-membered ring is bent towards the phenylalanine ligand (C18–C15–Ru1–O1 = −29°, C16–C14–Ru1–N1 = 30°, C17···C1 = 3.68 Å), so that the coordinated chloride is not hindered by the arene. Supramolecular association of **3a** differs remarkably from the strands of pseudo centric dimers observed for **1a**: the amidic $-NH_2$ group still employs both its hydrogens in two hydrogen bonds to the chloride anions (N2–H···Cl2 = 3.149(2) Å, 175.4(2)°; N2–H···Cl2$(1-x,\ y+1/2,\ -z)$ = 3.255(3) Å, 158.7(2)°), but these contacts are arranged in a chain generated by a two-fold screw rotation along ***b*** (Fig. 4). These chains are stabilized by the insertion of the water molecule that bridges the aminic–NH_2 and the amidic oxygen of pairs of consecutive molecules (N1–H···O1W$(x,\ y-1,\ z)$ = 2.906(4) Å, 122.5(2)°; O1W–H···O1 = 2.942(4) Å, 150(4)°), while the remaining NH hydrogen forms a weak hydrogen bond to the anionic chloride (N1–H···Cl2$(1-x,\ y-1/2,\ -z)$ = 3.349(3) Å, 148.0(2)°). Finally, the second water hydrogen interacts with an adjacent chain (O1W–H···Cl1$(2-x,\ y+1/2,\ 1-z)$ = 3.273(3) Å, 166(2)°). In **3a** all the hydrogen bond donors and acceptors are involved in the packing evidencing that

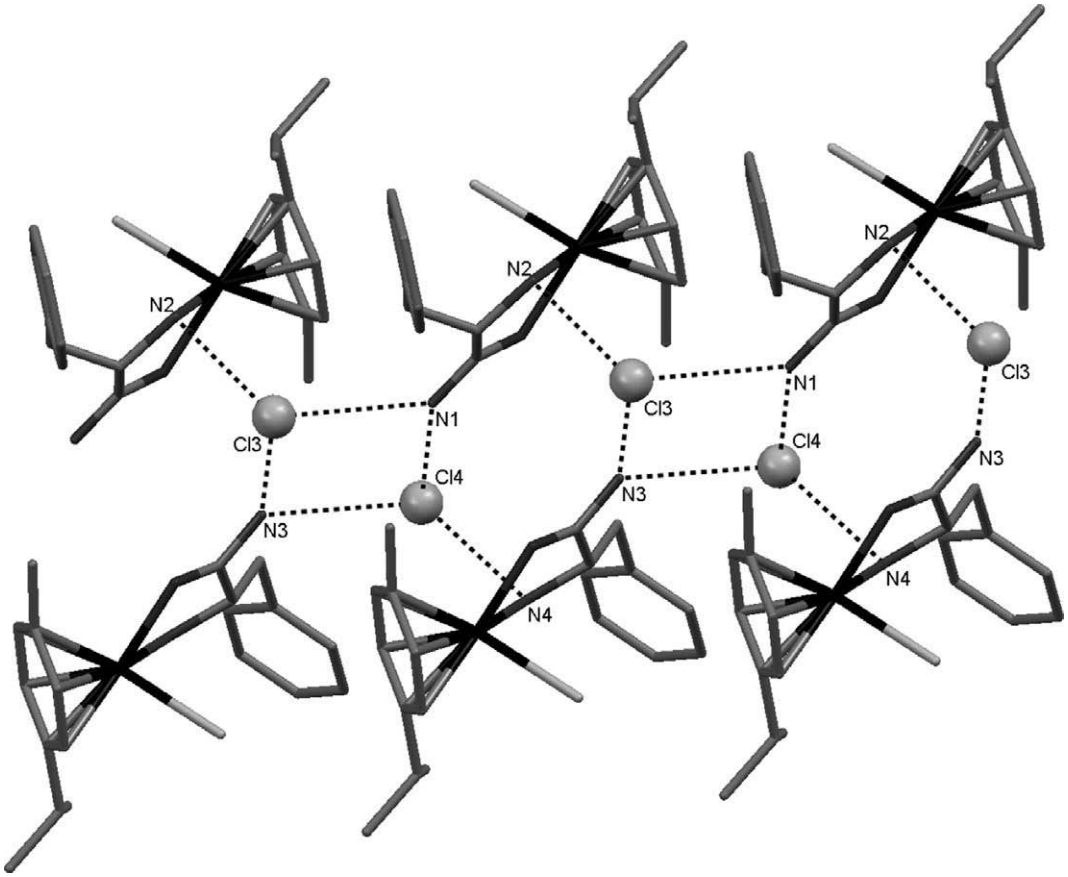

Fig. 2. Double strands organization in the crystal packing of **1a**, hydrogens omitted for clarity.

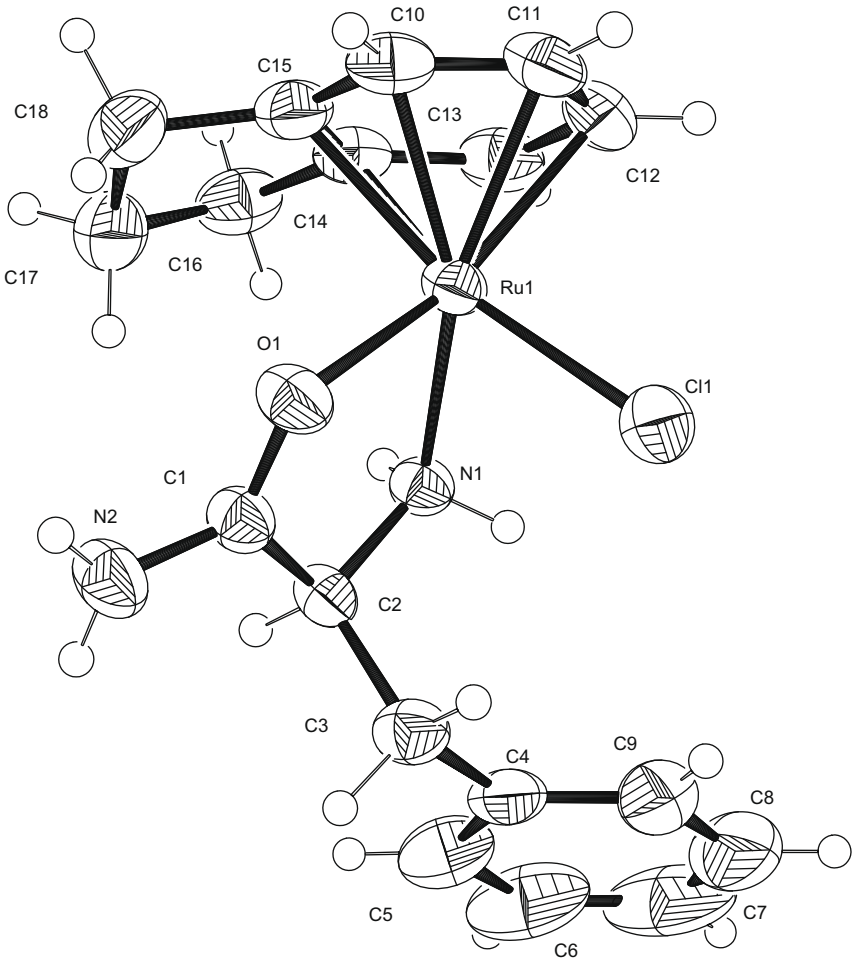

Fig. 3. Perspective view of the {Ru[(η^6-indane)(κ^2NO-phenylalanine amide]Cl}$^+$ cation in **3a**. Thermal ellipsoids at the 50% probability level.

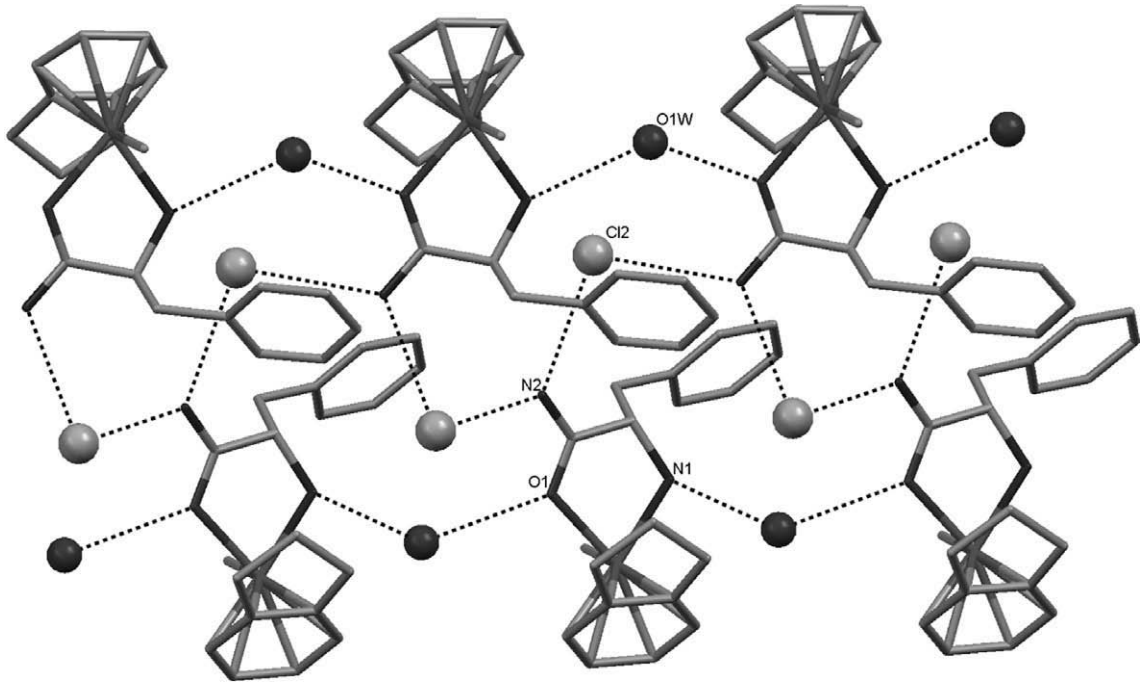

Fig. 4. Crystal packing of **3a**, hydrogens omitted for clarity.

hydration confers stability to the crystal structure of the single $R_{Ru}S_C$ isomer.

{Ru[(η^6-indane)proline amide]Cl}Cl (**4a**) is isolated as a single $S_{Ru}S_C$ isomer in the solid state (Fig. 5). The coordination geometry is in agreement with the one observed for **3a**, even if the two cations have opposite absolute configurations at the metal center (Table 1). The chelation ring is in this case less puckered then in the previously described compounds ($q2 = 0.13(1)$ Å^2,

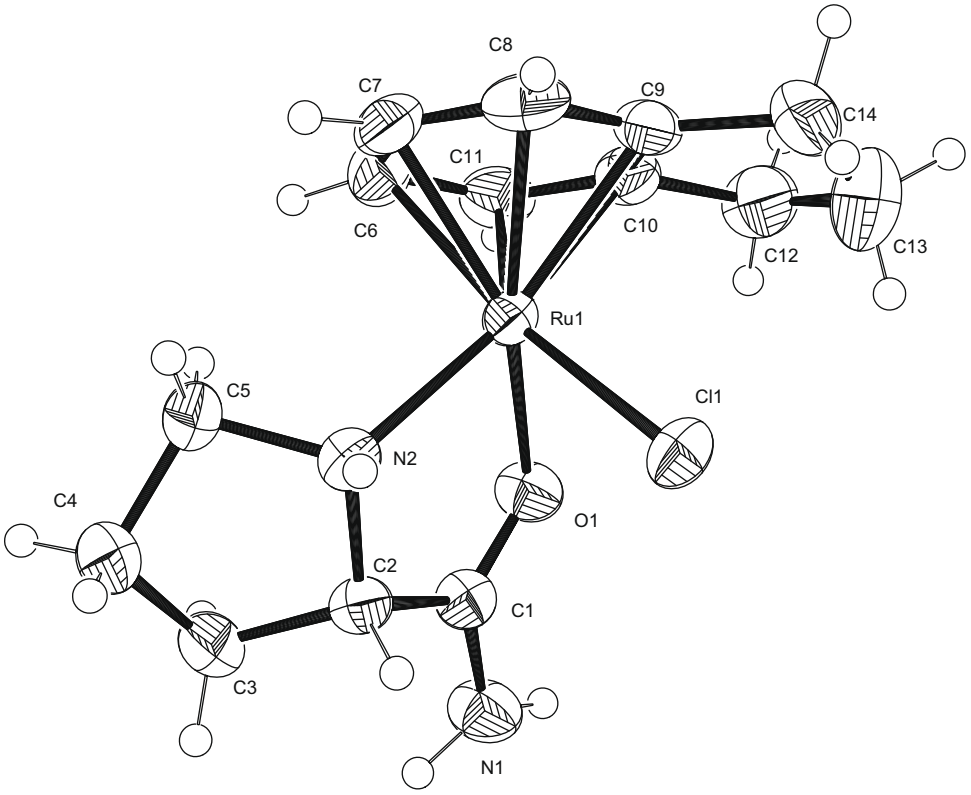

Fig. 5. Perspective view of the {Ru[(η^6-indane)(κ^2NO-proline amide)]Cl}$^+$ cation in **4a**. Thermal ellipsoids at the 50% probability level.

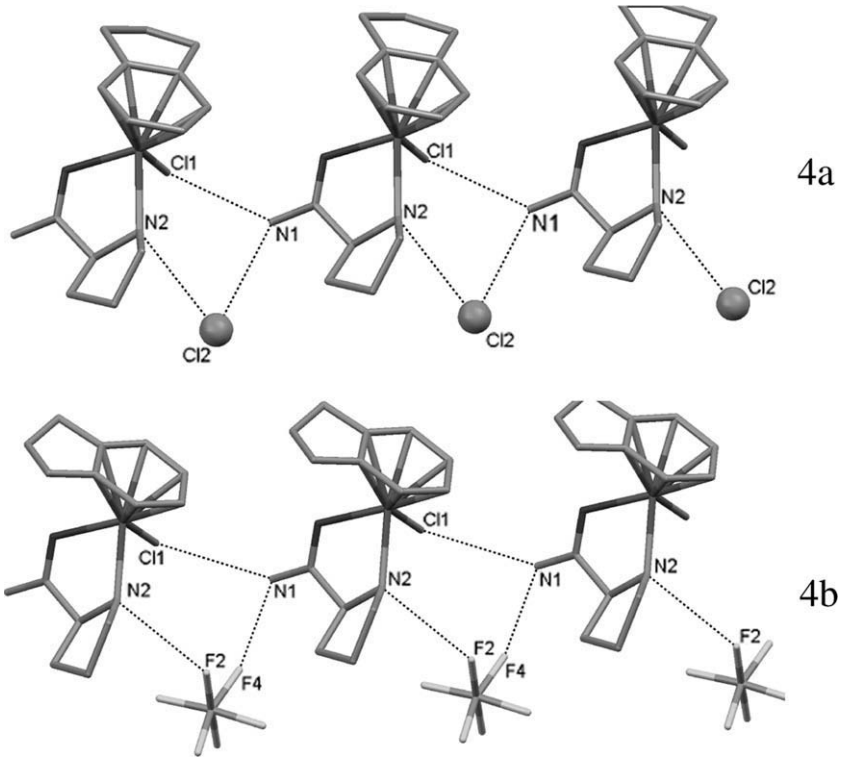

Fig. 6. Comparison of the solid state organization of **4a** (top) and **4b** (bottom), hydrogens omitted for clarity (N1–H···Cl1($x + 1, y, z$)): **4a** = 3.224(3) Å, 149(2)°; **4b** = 3.637(7) Å, 140.7(4)°); (N1–H···Cl2/F4: **4a** = 3.133(3) Å, 149(2)°; **4b** = 3.09(1) Å, 154.0(5)°; N2–H···Cl2/F2 ($x - 1, y, z$): **4a**: 3.419(2) Å, 149(3)°; **4b** = 3.133(7) Å, 153.9(3)°).

$\varphi 2 = -3(1)^\circ$). The absolute configuration at the metal implies that the proline five-membered cycle is oriented away from the chloride ligand; the indane aliphatic part by contrast points on the side of the halogen. The orientation of the indane ligand around the metal–arene bond is not strictly defined by intramolecular constraints, as it can be judged by observing that in the structure of {Ru[(η^6-indane) proline amide]Cl}PF_6 (**4b**) the cation presents the same configuration and coordination geometry than in **4a**, the only difference being the position of the indane aliphatic part, that in this case points to the oxygen atom of the L-proline amide ligand, evidencing also a high rotational thermal motion in the aromatic plane (see Supplementary data). **4b** is also isolated as the single $S_{Ru}S_C$ isomer in the solid state, and the coordination geometry is comparable with **4a**, the chelation ring being only slightly more puckered in **4b** ($q2 = 0.28(1)$ Å^2, $\varphi 2 = -9(1)^\circ$). Both for **4a** and **4b** the packing is based on the optimization of all possible hydrogen bonds between the —NH_2 and —NH donors and the chloride and anionic acceptors (Fig. 6). Namely, the interaction between —NH_2 and the coordinated chloride generates a translational chain along **c** (N1–H···Cl1($x+1$, y, z)): **4a** = 3.224(3) Å, 149(2)°; **4b** = 3.637(7) Å, 140.7(4)°), decorated by the Cl/PF_6 counteranions bonded to both NH_2 and NH (N1–H···Cl2/F4: **4a** = 3.133(3) Å, 149(2)°; **4b** = 3.09(1) Å, 154.0(5)°; N2–H···Cl2/F2 ($x-1$, y, z): **4a**: 3.419(2) Å, 149(3)°; **4b** = 3.133(7) Å, 153.9(3)°).

The observation of only a single diastereoisomer both in solution, once the crystals are dissolved, and in the solid state for complexes **4a-b,** compared to the presence of both isomers for **1** and **3**, would point to a more efficient stereoselectivity of prolineamide in keeping the chirality at the metal center unchanged. In fact, the inversion of the absolute configuration of the metal in **4** would imply that the five-membered cycle of the aminoamide would be rigidly oriented close to the chloride ligand, hinting at a steric destabilization of the $R_{Ru}S_C$ isomer. By contrast, actually this configuration has been observed in the only other example of crystal structure of a transition metal bound to a proline amide ligand {Rh[(Cp^*)Proline amide]Cl}Cl·$CHCl_3$ [23], where the bulky moiety of the proline points to the chloride, showing that this contact is feasible. Notably, also for this complex a single diastereoisomer was observed both in solution and in the solid. By contrast, the co-crystallization of both diastereoisomers of {Ir[(Cp^*)(*S*-prolinato)]Cl} [28] has also been observed.

3.3. Catalytic transfer hydrogenations

The reduction of carbonyl groups under hydrogen transfer conditions is a valuable alternative to the classic H_2-hydrogenation [29]. Half-sandwich Ru(II) complexes containing dinitrogen ligands have shown excellent activities and enantioselectivities in the reduction of prochiral ketones and imines, leading to secondary alcohols and amines with high optical purity [3b]. In our ongoing research program dedicated to the development of half-sandwich Ru(II) pre-catalysts based on amino-amide ligands, we have investigated the catalytic activity of the title complexes in the reduction of acetophenone in basic isopropanol. The optimization of the catalytic conditions, in terms of temperature and KOH/Ru molar ratio, has been performed by using complex **2b** as a model. As expected, the increase of the temperature brings to the increasing of the *tof* values, from 115 to 352 h^{-1}, after 30 min of reaction, on increasing the temperature from 20 to 82 °C, respectively. However, a decrease of the enantiomeric excess (from 79% to 68%) is also observed (see Supplementary data for the results obtained at intermediate temperatures). The best compromise between activity and enantioselectivity is reached at 30 °C, with an *ee* = 74%. This result is in good agreement with the result obtained by Faller with the same complex, although the Faller catalyst was applied at −24 °C reaching a conversion of 90% after 24 h of reaction. At a temperature of 30 °C two different KOH/Ru molar ratios, 2:1 and 4:1, have then been tested. The higher amount of base leads to a decrement of both conversions and enantiomeric excess. At 30 °C and with a KOH/Ru molar ratio of 2:1, the possibility of generating the catalyst *in situ* has also been tested. The collected results with preformed and *in situ* generated precatalyst **2b** are very close to each other, the largest difference observed over three independent runs being within 3%, both for *tof* and *ee*% values (compare entries 2 and 6 in Table 3). On the basis of the aforementioned results, all the subsequent catalytic tests have been conducted at a temperature of 30 °C, with a KOH/Ru molar ratio = 2:1, with preformed or *in situ* generated catalysts. The results are collected in Table 3. In all cases the reduction processes start immediately after the addition of the base without any induction period, with conversions higher than 50% after 30 min of reaction. The reactant solutions remain clear during the progress of the catalytic runs, decomposition becoming evident only maintaining the solution on stirring at conversions higher than 95%. In these cases, as expected, a decrement of the *ee*% was observed with time [3]. These observations, together with the found enantioselectivities, point out the homogeneous character of catalysis [30].

An inspection of the data collected in Table 3 indicates that the coordinated X and the uncoordinated Y anions do not affect the catalytic profile of the reactions, since only little variations of *tof* and *ee*% are observed for the reactions catalyzed by **1b**, **2b** and **5** (see entries 1, 2 and 7). The nature of the arene ligand does not influence greatly the *tof* values, the other ligands being the same, as can be inferred by comparing entries 1–3 and 2–4. The same comparison shows instead that *p*-cymene exerts a higher stereochemical control on the process with respect to indane, leading to higher *ee*s (compare entries 2 and 4). As regards the aminoamide ligand, L-prolineamide leads to 1-phenylethanol with higher optical purity, although higher *tof* values are reached with L-phenylalanine amide.

Table 3
Catalytic[a] results for the hydrogen transfer of acetophenone catalyzed by Ru-complexes.

Entry	Complex	Conversion(%)[b]	*ee*%[b]	*tof*(h^{-1})[c]
1	**1b**	97	30(*R*)	387
2	**2b**	59	74(*R*)	233
3	**3b**	97	17(*R*)	389
4	**4b**	70	54(*R*)	217
5	**2a**	54	76(*R*)	218
6	**2b**	60	75(*R*)	240
7	**5**	55	75(*R*)	222

[a] Conditions: [Ru] = 10^{-4}; Ru:KOH:acetophenone = 1:200:2; T = 30 °C.
[b] Determined by GC.
[c] Defined as: mole Ru x (mole acetophenone × h)$^{-1}$.

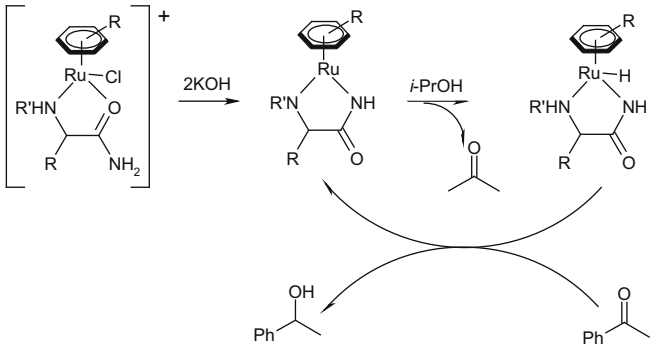

Scheme 3. Plausible mechanism for the transfer hydrogenation of acetophenone catalyzed by Ru-complexes.

The higher stereocontrol exerted by L-proline amide comes from the high geometric constrain imposed onto the Ru–N–C–C(O)–N chelation ring. The effect of the arene ligand on the enantioselectivity can be understood on taking into account that the hydrogen transfer reactions catalyzed by our complexes are governed by an outer sphere mechanism, as proposed by ESI(+)-MS analysis (*vide infra*). In fact, the origin of the enantioselectivity for half-sandwich Ru(II) complexes operating through an outer sphere mechanism, also referred as metal–ligand bifunctional catalysis, seems to reside in intermolecular C–H$\cdots\pi$ interactions occurring between the aromatic protons of the arene ligands and the phenyl group of acetophenone in the TS involved in the hydrogen transfer step [6,7,31]. The construction of such a type of pericyclic transition state could be hampered by the steric bulkiness of the indane ring, thus leading to a worse discrimination between the two enantiofaces of acetophenone.

In order to get more insights into the mechanism of the hydrogen transfer reactions, the methanol solutions of the complexes **1a** and **2a** previously analyzed by ESI(+)-MS, have been added of 2 equivalents of a KOH/*i*-PrOH solution (final KOH/Ru ratio = 2:1). The ESI(+) spectra show, in both cases, the signal corresponding to the potassate bis-amide 16e$^-$ ion {(η^6-arene)Ru[(κ^2-NN′)-bis amidato]K}$^+$as the most abundant cluster (m/z = 437 for **1a** and 387 for **2a**, respectively), with a residual cluster of the potassate amino-amidato ion {(η^6-arene)Ru[(κ^2-NN′)-amino amidato]ClK}$^+$ (m/z = 473 for **1a** and 423 per **2a**). The species detected by ESI(+)-MS are depicted in Scheme 2. The easy formation of the coordinatively unsaturated 16e$^-$ specie is strongly in favor of a metal–ligand bifunctional catalysis. The fact of not having observed any signal ascribable to the expected hydride species {(η^6-arene)Ru[(κ^2-NN′)-amino amidato]H}$^+$ finds its explanation in the high oxidation potential of methanale which makes methanol harder to oxidize than *i*-PrOH [32]. In fact, the hydrogen transfer of acetophenone conducted in MeOH in the presence of **2a** under the conditions reported in Table 3, proceeded very sluggishly, leading to traces of 1-phenylethanol after 24 h of reaction.

In analogy with what seen with amino amidato complexes, and on the basis of the collected experimental evidences, a plausible mechanism can then be advanced (see Scheme 3): one equivalent of KOH is necessary in order to deprotonate the amide function transforming the starting complexes in the corresponding amino amidato complexes {(η^6-arene)Ru[(κ^2-NN′)-amino amidato]Cl}. These react with the second equivalent of KOH giving rise to the 16e$^-$ bis-amidato intermediates {(η^6-arene)Ru[(κ^2-NN′)-bis amidato]}, which by interaction with *i*-PrOH generate acetone and the hydride intermediate {(η^6-arene)Ru[(κ^2-NN′)-amino amidato]H}$^+$. This reacting with acetophenone gives the 16e$^-$ bis amidato intermediate back eliminating the desired 1-phenylethanol.

4. Conclusions

In the present work we have shown the synthesis and the full characterization of a series of new half-sandwich Ru(II) complexes containing two different aminoacid amides, to say L-proline amide and L-phenylalanine amide, and two different arene rings, such as *p*-cymene and indane. By X-ray, NMR and CD data it has been possible to establish the metal configuration in most of the cases, as well as the configuration stability shown by the complexes once brought in solution. The two amino amide ligands have shown different degrees of stereochemical control, with L-proline amide leading always to higher diastereomeric excesses. An important role on the metal configurational stability seems to be played also by the arene ring. In fact, the combination L-proline amide with indane leads to configurationally stable complexes, which once isolated as pure diastereoisomers in the solid state, do not show any degree of epimerization in solution. On the contrary, the iodide complex **5**, arising from the combination of L-proline amide with *p*-cymene, although isolated as a single isomer in crystalline form, shows epimerization in methanol solution. The ability of **5** to crystallize as a single diastereoisomer cannot be imputed to the presence of the iodide ligand, since co-crystallization of the two opposite diastereoisomers has been observed also with iodo-complexes of Ru(II) [23,33].

The isolated complexes are active catalysts in the reduction of acetophenone under hydrogen transfer conditions. The most enantioselective catalysts are those containing L-proline amide and *p*-cymene, leading to enantioselectivity up to 76% in favor of the *R* isomer of 1-phenylethanol. On the basis of ESI(+)-MS data the catalytic processes seem governed by a metal–ligand bifunctional mechanism.

Acknowledgments

The authors thank Centro Interdipartimentale di Misure "G. Casnati" of the University of Parma for the instrument facilities. Dr Lisa Elviri (University of Parma) is thanked for the ESI(+)-MS spectra recording, while Dr Tiziana Chiodo (University of Parma) is thanked for X-ray data collection.

Appendix A. Supplementary data

CCDC 727129, 727130, 727131, 727132 and 727133 contain the supplementary crystallographic data for complexes (**1a**), (**3a**), (**4a**), (**4b**), (**5**). These data can be obtained free of charge from The Cambridge Crystallographic Data Centre via www.ccdc.cam.ac.uk/data_request/cif.

Supplementary data associated with this article can be found, in the online version, at doi:10.1016/j.jorganchem.2009.05.010.

References

[1] (a) Y.-F. Han, Y.-J. Lin, L.-H. Weng, H. Berke, G.-X. Jin, Chem. Commun. (2008) 350–352;
(b) K. Severin, Chem. Commun. (2006) 3859–3867.
[2] (a) Y.K. Yan, M. Melchart, A. Habtemariam, P.J. Sadler, Chem. Commun. (2005) 4764–4776;
(b) C.A. Vock, C. Scolaro, A.D. Phillips, R. Scopelliti, G. Sava, P.J. Dyson, J. Med. Chem. 49 (2006) 5552–5561;
(c) S.J. Dougan, M. Melchart, A. Habtemariam, S. Parsons, P.J. Sadler, Inorg. Chem. 45 (2006) 10882–10894;
(d) A. Habtemariam, M. Melchart, R. Fernández, S. Parsons, I.D.H. Oswald, A. Parkin, F.P.A. Fabbiani, J.E. Davidson, A. Dawson, R.E. Aird, D.I. Jodrell, P.J. Sadler, J. Med. Chem. 49 (2006) 6858–6868.
[3] (a) J. Takehara, S. Hashiguchi, A. Fujii, S. Inoue, T. Ikariya, R. Noyori, Chem. Commun. (1996) 233–234;
(b) R. Noyori, S. Hashiguchi, Acc. Chem. Res. 30 (1997) 97–102;
(c) D.A. Alonso, D. Guijarro, P. Pinho, O. Temme, P.G. Andersson, J. Org. Chem. 63 (1998) 2749–2751;
(d) S. Hashiguchi, A. Fujii, J. Takehara, T. Ikariya, R. Noyori, J. Am. Chem. Soc. 117 (1995) 7562–7563;
(e) K. Matsumura, S. Hashiguchi, T. Ikariya, R. Noyori, J. Am. Chem. Soc. 119 (1997) 8738–8739.
[4] T. Ohta, S. Nakahara, Y. Shigemura, K. Hattori, I. Furukawa, Chem. Lett. (1998) 491–492.
[5] T. Ohta, S. Nakahara, Y. Shigemura, K. Hattori, I. Furukawa, Appl. Organomet. Chem. 15 (2001) 699–709.
[6] M. Yamakawa, I. Hisashi, R. Noyori, J. Am. Chem. Soc. 122 (2000) 1466–1478.
[7] M. Yamakawa, I. Yamada, R. Noyori, Angew. Chem., Int. Ed. 40 (2001) 2818–2821.
[8] J.W. Faller, A.R. Lavoie, Organometallics 20 (2001) 5245–5247.
[9] (a) H.Y. Rhyoo, Y.A. Yoon, H.J. Park, Y.K. Chung, Tetrahedron Lett. 42 (2001) 5045–5048;
(b) H.R. Rhyoo, H.J. Park, Y.K. Chung, Chem. Commun. (2001) 2064–2065;
(c) H.Y. Rhyoo, H.J. Park, W.H. Suh, Y.K. Chung, Tetrahedron Lett. 43 (2002) 269–272.
[10] (a) A. Bøgevig, I.M. Pastor, H. Adolfsson, Chem. Eur. J. 10 (2004) 294–302;
(b) I.M. Pastor, P. Västilä, H. Adolfsson, Chem. Commun. (2002) 2046–2047;
(c) I.M. Pastor, P. Västilä, H. Adolfsson, Chem. Eur. J. 9 (2003) 4031–4045;
(d) A.B. Zaitsev, H. Adolfsson, Org. Lett. 8 (2006) 5129–5132.

[11] (a) P. Pelagatti, A. Bacchi, F. Calbiani, M. Carcelli, L. Elviri, C. Pelizzi, D. Rogolino, J. Organomet. Chem. 690 (2005) 4602–4610;
(b) P. Pelagatti, M. Carcelli, F. Calbiani, C. Cassi, L. Elviri, C. Pelizzi, U. Rizzotti, D. Rogolino, Organometallics 24 (2005) 5836–5844;
(c) A. Bacchi, M. Balordi, R. Cammi, L. Elviri, C. Pelizzi, F. Picchioni, V. Verdolino, K. Goubitz, R. Peschar, P. Pelagatti, Eur. J. Inorg. Chem. (2008) 4462–4473.
[12] M.A. Bennet, T.N. Huang, T.W. Matheson, A.K. Smith, Inorg. Synth. (1982) 74–78.
[13] L. Vielille-Petit, B. Therrien, G. Süss-Fink, Acta Cryst. E58 (2002) m656.
[14] (a) SAINT: SAX, Area Detector Integration, Siemens Analytical Instruments INC., Madison, Wisconsin, USA;
(b) G. Sheldrick, SADABS: Siemens Area Detector Absorption Correction Software, 1996, University of Goettingen, Germany.
[15] A. Altomare, M.C. Burla, M. Cavalli, G. Cascarano, C. Giacovazzo, A. Gagliardi, A.G. Moliterni, G. Polidori, R. Spagna, Sir97: A New Program For Solving and Refining Crystal Structures, Istituto di Ricerca per lo Sviluppo di Metodologie Cristallografiche CNR, Bari, 1997.
[16] G. Sheldrick, Shelxl97, Program for Structure Refinement, University of Goettingen, Germany, 1997.
[17] L.J. Farrugia, J. Appl. Cryst. 32 (1999) 837–838.
[18] M. Nardelli, J. Appl. Cryst. 28 (1995) 659.
[19] (a) F.H. Allen, O. Kennard, R. Taylor, Acc. Chem. Res. 16 (1983) 146–153;
(b) I.J. Bruno, J.C. Cole, P.R. Edgington, M. Kessler, C.F. Macrae, P. McCabe, J. Pearson, R. Taylor, Acta Crystallogr. B58 (2002) 389–397.
[20] W. Hoffmuller, K. Polborn, J. Knizek, H. Noth, W. Beck, Zeit. Anorg. Allg. Chem. 623 (1997) 1903–1911.
[21] R. Krämer, M. Maurus, R. Bergs, K. Polborn, K. Sünkel, B. Wagner, W. Beck, Chem. Ber. 126 (1993) 1969–1980.
[22] (a) D. Carmona, A. Mendoza, F.J. Lahoz, L.A. Oro, M.P. Lamata, E. San Jose, J. Organomet. Chem. 396 (1990) C17–C21;
(b) L.C. Carter, D.L. Davies, K.T. Duffy, J. Fawcett, D.R. Russell, Acta Cryst. C50 (1994) 1559–1561;
(c) D. Carmona, F.J. Lahoz, R. Atencio, L.A. Oro, M.P. Lamata, F. Viguri, E. San Jose, C. Vega, J. Reyes, F. Joó, A. Kathó, Chem. Eur. J. (1999) 1544–1564;
(d) A. Kathó, D. Carmona, F. Viguri, C.D. Remacha, J. Kovács, F. Joó, L.A. Oro, J. Organomet. Chem. 593–594 (2000) 299–306.
[23] (a) H. Brunner, M. Weber, M. Zabel, Coord. Chem. Rev. 242 (2003) 3–13;
(b) H. Brunner, M. Weber, M. Zabel, T. Zwack, Angew. Chem., Int. Ed. 42 (2003) 1859–1862.
[24] (a) A.J. Davenport, D.L. Davies, J. Fawcett, D.R. Russell, J. Chem. Soc., Dalton Trans. (2004) 1481–1492;
(b) H. Brunner, R. Oeschey, B. Nuber, J. Chem. Soc., Dalton Trans. (1996) 1499–1508;
(c) S.K. Mandal, A.R. Chakravarty, J. Chem. Soc., Dalton Trans. (1992) 1627–1633.
[25] (a) L. He, Z. Tang, L.-F. Cun, A.-Q. Mi, Y.-Z. Jiang, L.-Z. Gong, Tetrahedron 62 (2006) 346–351;
(b) H.-M. Guo, L.-F. Cun, L.-Z. Gong, A.-Q. Mi, Y.-Z. Jiang, Chem. Commun. (2005) 1450–1452.
[26] D. Cremer, J.A. Pople, J. Am. Chem. Soc. 75 (1997) 1354–1358.
[27] C.P. Brock, J.D. Dunitz, Chem. Mater. 6 (1994) 1118–1127.
[28] (a) R. Kramer, K. Polborn, H. Wanjek, I. Zahn, W. Beck, Chem. Ber. 123 (1990) 767;
(b) D. Carmona, A. Mendoza, F.J. Lahoz, L.A. Oro, J. Organomet. Chem. 396 (1990) C17–C21.
[29] J.G. de Vrieze, C.J. Elsevier, Handbook of Homogeneous Hydrogenation, Wiley-VCH, Weinheim, 2007.
[30] J.A. Widegren, R.G. Finke, J. Mol. Catal. A: Chem. 198 (2003) 317–341.
[31] R. Noyori, M. Yamakawa, S. Yashiguchi, J. Org. Chem. 66 (2001) 7931–7944.
[32] H. Adkins, R.M. Elofson, A.G. Rossow, C.C. Robinson, J. Am. Chem. Soc. 71 (1949) 3622–3629.
[33] H. Brunner, T. Zwack, M. Zabel, W. Beck, A. Böhm, Organometallics 22 (2003) 1741–1750.